



# Measurement of environmental parameters in polar regions based on a ubiquitous sensor network



Namyi Chae<sup>a,c</sup>, Heekwon Yang<sup>b</sup>, Bang Yong Lee<sup>c</sup>, Chankil Lee<sup>b,\*</sup>

<sup>a</sup> Civil & Environmental Engineering, Yonsei University, 50 Yonsei-ro, Seodaemun-gu, Seoul 03722, Republic of Korea

<sup>b</sup> Department of Electronics and Communications Eng., Hanyang University ERICA Campus, 55 Hanyangdaehak-ro, Sangrok-gu, Ansan, Gyeonggi-do 15588, Republic of Korea

<sup>c</sup> Arctic Research Center, Korea Polar Research Institute, 26 Songdomirae-ro, Yeosu-gu, Incheon 21990, Republic of Korea

## ARTICLE INFO

### Article history:

Received 18 July 2014

Received in revised form 28 October 2015

Accepted 2 November 2015

Available online 11 November 2015

### Keywords:

Permafrost

Active layer

Ubiquitous sensor network

Network scalability

Spatial variation

## ABSTRACT

To estimate the spatial variation of soil CO<sub>2</sub> flux in a permafrost region, major environmental parameters were measured and analyzed using the proposed ubiquitous sensor network-based remote monitoring system (U-RMS). The use of techniques for power-efficient operation and network scalability that enable long-term use of a wireless sensor network (WSN) that can be deployed reliably and widely is described. The temporal and spatial variations in air temperature (Ta) and relative humidity (RH) near the surface at 16 locations and soil temperature (Ts) and soil water content (SWC) at 10 locations were measured to monitor the active permafrost layer in Alaska from September 2012 to January 2013 and from July to September 2013. The temporal variations in environmental parameters in the soil and near the surface depended on the thawing and freezing of the snow cover in the permafrost regions. The spatial patterns of Ts in the three periods were not similar because of the heterogeneous distribution of snow coverage and depth in winter. On the other hand, the spatial patterns of Ts and SWC had a negative relationship during summer. The spatial variations in Ts and SWC showed a high coefficient of variation (CV) that ranged from 20% to 40%, while the CV of Ta and RH was within 5% except in winter due to the spatially heterogeneous snow cover. The relationship between CO<sub>2</sub> efflux and Ts or SWC in 2012, which had a high CV, was examined to estimate the soil CO<sub>2</sub> efflux in 2013. The Ts explained ~60% (soil CO<sub>2</sub> efflux = 0.066 × exp<sup>0.1443 × Ts</sup>, R<sup>2</sup> 0.59) of the variation in soil CO<sub>2</sub> efflux in a temperature range of 3 to 8 °C. Therefore, the soil CO<sub>2</sub> efflux in 2013 was estimated in the range of 0.08 mg m<sup>-2</sup> s<sup>-1</sup> to 0.47 mg m<sup>-2</sup> s<sup>-1</sup>, and average CV was 25%. Using the camera sensor, the growth of vegetation and the operating appearance of the remote WSN were also monitored. In the long term, measurement of temporal and spatial variations in environmental parameters, based on U-RMS, is expected to contribute to the understanding of the carbon and water cycles in permafrost.

© 2015 The Authors. Published by Elsevier B.V. This is an open access article under the CC BY-NC-ND license (<http://creativecommons.org/licenses/by-nc-nd/4.0/>).

## 1. Introduction

Permafrost regions occupy about one-quarter of the land surface of the northern hemisphere (Pewe, 1983; Zhang et al., 2000). Long-term monitoring of temperature and moisture content on or within an active layer and active layer thickness and spatial variability is essential to investigate the response of permafrost to climate change. These environmental aspects of permafrost support an understanding of the cycle of greenhouse gases as the controlling parameters of the biological process (Oechel and Vourlitis, 1994; Vourlitis et al., 1993). Soil CO<sub>2</sub> efflux is controlled primarily by soil temperature and soil water content. Soil temperature explains the variation in soil respiration in various ecosystems as the most important factor controlling soil carbon emission

(Boone et al., 1998; Lloyd and Taylor, 1994), while soil water content plays a positive or negative role depending on the water conditions (Davidson et al., 2000; Rey et al., 2002; Swanson and Flanagan, 2001). Especially in permafrost, the spatial distribution of both parameters within tens of meters is unpredictable because of the extent of thawing and variation in the active layer during the thawing season. Therefore, spatial variations in soil temperature and soil water content are very important in investigating soil CO<sub>2</sub> flux and will be used in modeling carbon emission in the tundra.

To understand the changing properties of permafrost in the tundra ecosystem, long-term continuous measurements must be conducted. However, there are limitations in site accessibility, data transfer, and the supply of electric power according to the weather conditions and the topographic and geographic characteristics at the high latitudes of the tundra.

Environmental monitoring has been conducted to overcome the difficulties of using various techniques and methods (e.g., sensor

\* Corresponding author. Tel.: +82 31 400 5294; fax: +82 31 415 9183.

E-mail addresses: [cnamyi@yonsei.ac.kr](mailto:cnamyi@yonsei.ac.kr) (N. Chae), [hkyang77@hanyang.ac.kr](mailto:hkyang77@hanyang.ac.kr) (H. Yang), [bylee@kopri.re.kr](mailto:bylee@kopri.re.kr) (B.Y. Lee), [cklee@hanyang.ac.kr](mailto:cklee@hanyang.ac.kr) (C. Lee).

networking, wireless sensing, and acoustic sensing) in permafrost (Albert et al., 2008; Kotovirta et al., 2011; Vilajosana et al., 2011). As the wireless sensor network (WSN) technologies provide many advantages, such as low power consumption, low cost, easy installation, and network reliability and scalability, they have been widely used for real-time monitoring of environmental change for prevention of disasters; automation in various fields, such as in factories, agriculture, and homes; and collection of environmental data for research purposes (Gill et al., 2009; Gungor and Hancke, 2009; Sardini and Serpelloni, 2011; See et al., 2012; Spacek et al., 2013; Wang and Liao, 2006; Whelan et al., 2009).

In micrometeorology research, the system for measuring spatial variation in the micrometeorological parameters of a wide field has a weak infrastructure (e.g., electricity and communication). Therefore, a ubiquitous sensor network-based remote monitoring system (U-RMS) was used to overcome this problem. This study has two main objectives. First, we present the U-RMS for collecting and managing the environmental data of air temperature (Ta) and relative humidity (RH) of the near-surface, soil temperature (Ts), soil water content (SWC), and camera images from the WSN deployed in Council, Alaska. Second, we performed spatial and temporal analyses of the environmental parameters at the micrometeorological measurement site (i.e., the chamber and eddy flux tower system). Ta, RH, Ts, and SWC play important roles in the tundra ecosystem as controlling parameters of the carbon cycle.

## 2. Description of the ubiquitous sensor network-based remote monitoring system (U-RMS)

The U-RMS is a real-time, two-way communication observation system that collects environmental data from polar regions that are not easily accessible. The U-RMS is basically a WSN system that uses an Iridium satellite network (ISN) backbone, as shown in Fig. 1. Efficient data transmission from the remote WSN to a local monitoring center was achieved through the use of two types of ubiquitous sensor network (USN) gateways equipped with an Iridium modem. For use on

the local PC, an application software program was developed for status determination and parameter setting of the WSN and for management of the climate and image data collected from the remote WSN.

### 2.1. Wireless sensor network (WSN)

The WSN consists of sensor nodes, which operate in sleep and wakeup modes, and a gateway that performs protocol conversion between the WSN and the ISN. This section describes the components used in a sensor node, its usable lifetime, and the scalability of a WSN.

#### 2.1.1. Sensor nodes

One of the measurement or image sensors is combined with a ZigBee radio control module (RCM) in a sensor node that acts as a sleepy ZigBee end device (ZED) (ZigBee Standard Organization, 2007). The RCM uses EM357 (Ember, USA), its receiver sensitivity is normally  $-100$  dBm, and it performs at a 1% packet error rate for a 20-byte packet. The external power amplifier RF6525 (RFMD, USA) is added to extend the communication range by controlling the transmission power. The ZigBee RCM in the USN gateway takes charge of the network management, as a ZigBee coordinator (ZC) device.

Each sensor node is battery (3.6 V–19 AH Lithium XL-205F, Xenenergy, Korea)-powered and designed to operate for at least one year. Its network components must be designed to minimize power consumption for its long-term operation in unpowered regions. The sleep and wakeup intervals, which are remotely controllable, determine the battery life and how often and for how long measurements can be made. With the sleep-wakeup algorithm, sensor nodes will consume only several  $\mu$ A when the radio is in sleep mode. To estimate the operating life-time of sensor nodes, the current consumptions when the sensing data were transferred to the USN gateway were measured for the soil, near-surface, and image sensor nodes, respectively. Based on these measurements, the possible number of measurements/days for a one-year operation was determined to be 12,686 and 71,292 for the soil sensor and the near-surface sensor, respectively. The image sensors

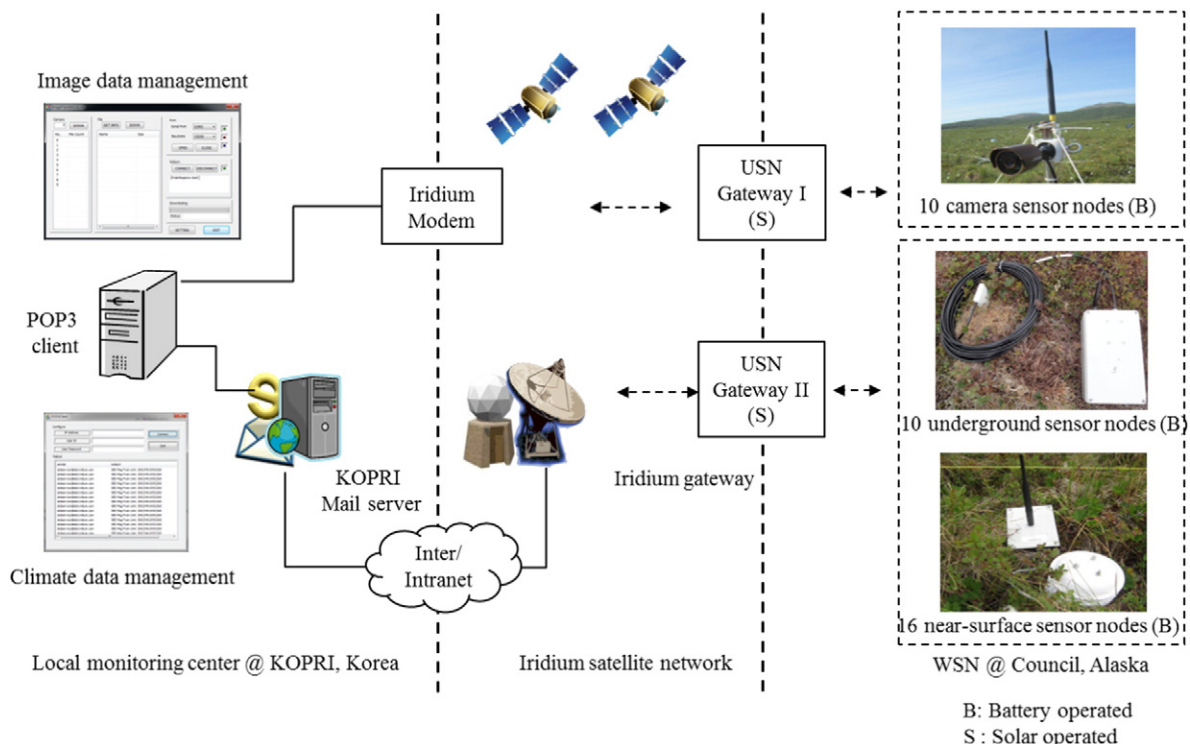


Fig. 1. Ubiquitous sensor-network-based remote monitoring system (U-RMS) architecture.

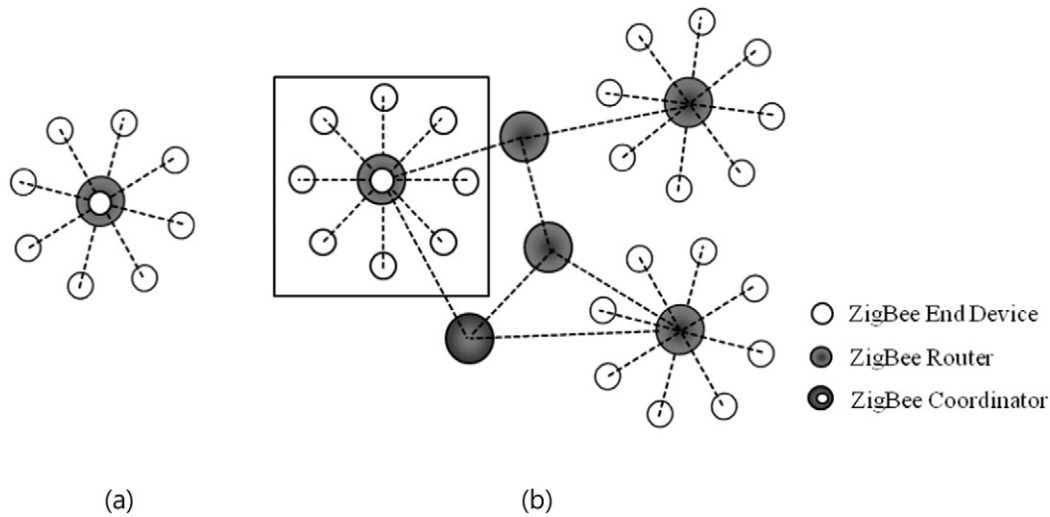


Fig. 2. Network topology for the (a) star and (b) hybrid mesh.

were shown to be able to capture 50 images in one day. The analysis included temperature de-rating at  $-30\text{ }^{\circ}\text{C}$ , at which point the battery capacity drops to 30% of its nominal capacity.

#### 2.1.2. Network scalability

Using the two types of devices, ZC and sleepy ZED, the WSN was deployed with a star topology (Fig. 2). Prior to the deployment, the communication range of the external-power-added-RCM was tested in a line of sight environment. Using a 17-dBm transmission power, the average received signal strength (RSS) at a 500 m distance was measured as  $-88\text{ dBm}$ . No communication error occurred in the 1000 packet transmission trials. During the observation period after deployment, the average RSS was  $-55\text{ dBm}$  without any packet loss. Based on these experimental results, the deployment area can be extended up to  $500\text{ m} \times 500\text{ m}$ .

#### 2.2. Ubiquitous sensor network (USN) gateways

To convert the communication protocol of the WSN to that of the ISN, a USN gateway is used, as shown in Fig. 3. Since the measured data are as small as 240 bytes per measurement, the Iridium modem (9602-N, NAL Research Co., USA) in a short-burst data (SDB) service was used because it consumes relatively little power and transfers small amounts of data more efficiently than does the dial-up data (DUD) service that is associated with circuit-switched data calls. To

transfer the image data, the Iridium modem (A3LA-X, NAL Research Co.) in the DUD service was used, because it provides a better transmission rate without the need for the terrestrial ISN gateway. In case data transfer via the ISN is not possible, a 16 GB backup storage is mounted at the USN gateway to prevent loss of the collected data from the WSN.

Since the USN gateway operates for two seconds every 10 min, its average power consumption is 0.83 W. Assuming three hours of sunlight in one day and 40% loss of output power, a solar panel that generates 20 W of power was used, which is larger than the calculated 11-W power need. Assuming that there could be six sunless days and a 25% charging loss, 13 AH was required, so a 12 V, 60 AH rechargeable battery was chosen. Taking into consideration the polar nights with no midnight sun and the 165-mA standby current consumption, a backup 12 V, 600 AH Li-battery was used.

To collect and manage the measurements and the image data, two separate application software programs were developed. The application software for the measurement data, the post office protocol version 3 (POP3) client, enables downloading of the data in the Korea Polar Research Institute (KOPRI) mail server onto the hard disk of a local PC. The sensing interval, transfer period, and backup interval can also be configured. Using the application software for image data, the shooting time, resolution, and compression rate of a camera can be configured directly through the Iridium DUD modem connected to a local PC via RS 232C. In the application window, the image data to be remotely transferred to the local PC can be selected and imported.

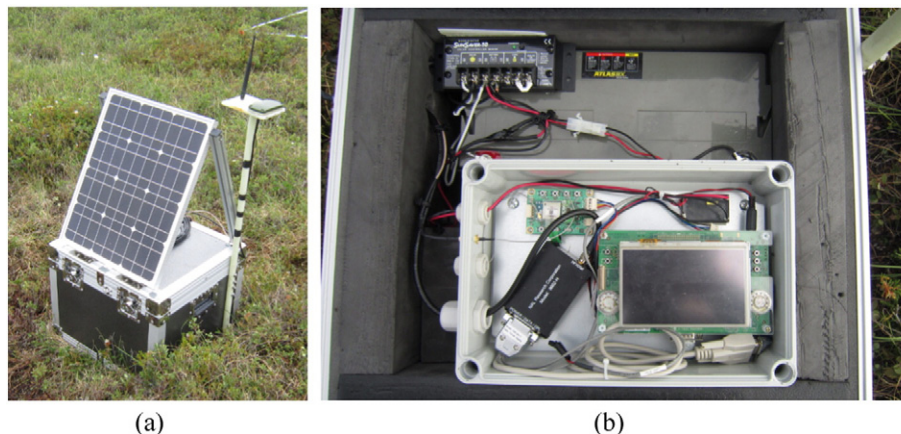


Fig. 3. Installation of the gateway for (a) complete assembly and (b) internal components.

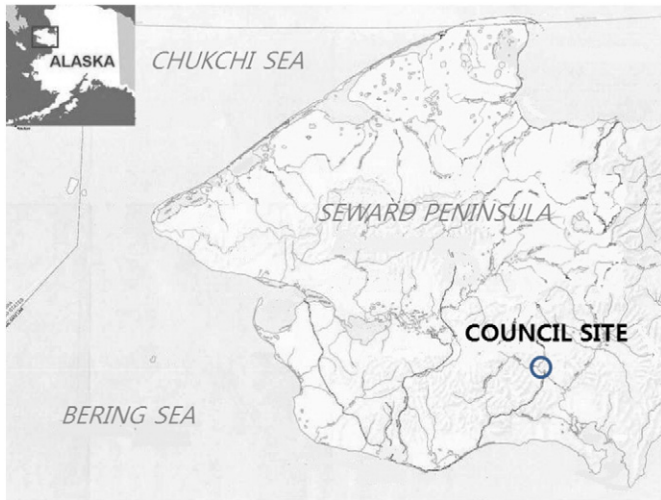


Fig. 4. Measurement site in Council (64°50.63' N, 163°42.64' W), Seward Peninsula, Alaska.

3. Materials and methods

3.1. The study site

This study was conducted in Council, Alaska (64° 50.63' N, 163° 42.64' W), on the Seward Peninsula (Fig. 4). The site contains vascular plants (e.g., *Erophorum scheuchzeri* and *Betula nana*), moss (e.g., *Sphagnum lenese pohle* and *Sphagnum russowii* Warnst), and lichen (e.g., *Cladonia stellaris*). The vegetation type is mainly tussock, underlain by soil (i.e., Histic Cryosols). The annual Ta ranges from -30 to 20 °C; the predominant wind directions are north and north-west; the wind speed generally ranges from 2 to 6 m s<sup>-1</sup>; and the average maximum snow depth has been about 0.7 m from February to April over the last 10 years, according to the meteorological data of the International Arctic Research Center of the University of Alaska, Fairbanks. The depth of the active layer was measured at a maximum of ~0.6 m in early September in 2012 and 2013. The automated chamber system and the eddy covariance method system have been used on this site to investigate CO<sub>2</sub> exchange between soil, vegetation, and atmosphere.

Table 1  
Locations, depth, and periods of environmental parameters.

Parameter	Location (No.)	Depth (m)	Period
Ta	1–16	0.1	Periods I, II, III
RH	1–16	0.1	Periods I, II, III
Ts	1–10	0.1	Periods I, II
SWC	1, 3, 5, 6, 7, 8, 9, 10 / 2, 4	0.1 / 0.3	Periods III
	1, 3 / 2, 4, 5, 6, 7, 8, 9, 10	0.1 / 0.1 – 0.4	Periods I, II
	1, 3, 5, 6, 7, 8, 9, 10 / 2, 4	0.1 / 0.3	Periods III

The chamber method using an infra-red gas analyzer is used to measure soil CO<sub>2</sub> efflux over soil surface (Nay et al., 1994). The eddy covariance method using sonic anemometers and infrared gas analyzers is used to measure energy flux and CO<sub>2</sub> flux in the surface boundary layer (Foken et al., 2012).

3.2. Measurements

The study period from 13 September 2012 to 25 September 2013 was divided into three sub-periods: period I (13 September to 2 November 2012), period II (3 November 2012 to 27 January 2013), and period III (18 July 2013 to 25 September 2013). The measurement of Ta, RH, Ts and SWC was conducted in a 100 m × 100 m plot that included the site of the automated chamber system (Fig. 5). Ta, RH, Ts, and SWC were measured in areas with representative vegetation (Table 1). Three kinds of sensor were used, one measuring Ta and RH (SHT71, Sensirion, Switzerland), another Ts and SWC (CS650L, Campbell Scientific, Inc., USA), and a third capturing images (SCAM-30, Hanjin, Korea). The major specifications of the sensors and the camera are described in Table 2.

Ta and RH were simultaneously measured 0.1 m above the ground at 16 locations using SHT71, which was equipped with a radiation shield during periods I–III. Ta and RH were measured in the air in the snow-free season and in the snow layer in the snow-covered season because the sensor was covered by snow in winter.

Ts and SWC were also simultaneously measured at 10 locations using CS650L. CS650L is a probe type of 30 cm in length for measuring SWC and Ts at the same time. SWC was detected over the whole probe length but Ts was detected only at the top of the probe. For periods I and II, the sensors were installed horizontally in two locations (Nos. 1 and 3) and vertically in eight locations (Nos. 2, 4, 5, 6, 7, 8, 9, and 10) in the soil. The Ts was measured at a depth of about 0.1 m in 10 locations, and SWC was measured at a depth of about 0.1 m in two locations (Nos. 1 and 3) and in the 0.1–0.4 m soil layer in the other eight locations (Nos. 2, 4, 5, 6, 7, 8, 9, and 10) for periods I and II. However, Ts at the two locations (Nos. 3 and 7) was not recorded because of communication errors due to water leakage. For period III, all sensors were installed horizontally, and Ts and SWC were measured at a depth of about 0.3 m at two locations (Nos. 2 and 4) and at a depth of about 0.1 m in the other eight locations (Nos. 1, 3, 5, 6, 7, 8, 9, and 10). To monitor the phenology, environment, and operation of the measurement systems during the study period, 10 cameras were installed inside

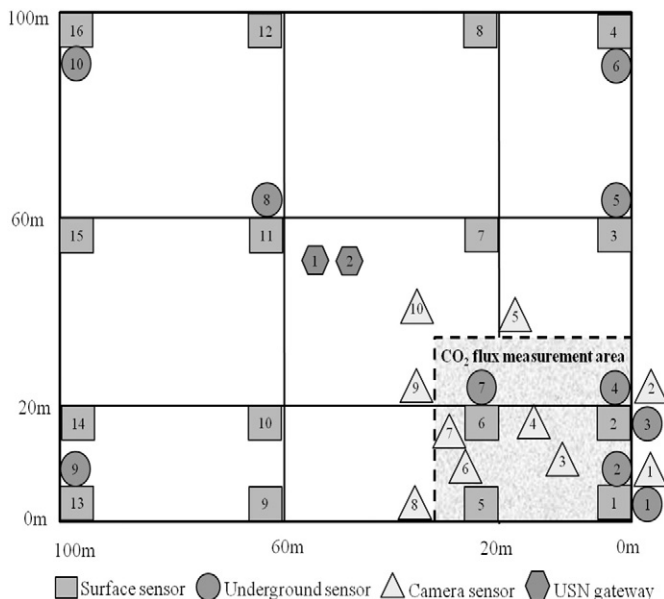


Fig. 5. Sensor positions in the measurement plot (100 m × 100 m).

Table 2  
Major specification of measurement sensors and camera.

Sensor	Operating range	Accuracy	Precision	
CS650	Volumetric water contents	5–50%	± 3% VWC <sup>a</sup>	<0.05%
	Temperature	-10–70 °C	± 0.5 °C <sup>b</sup>	± 0.02 °C
SHT71	Relative humidity	0–100% RH	± 3% RH	± 0.1% RH
	Temperature	-40–123.8 °C	± 0.4 °C	± 0.1 °C
SCAM-30	Image sensor	-10–70 °C	0.3 M pixel (VGA), JPEG <sup>c</sup> , 120° view angle, 45 dB SNR	

<sup>a</sup> Typical in mineral soils where electrical conductivity ≤ 3 dS/m.

<sup>b</sup> For probe body buried in soil.

<sup>c</sup> Variable compression rate of 16 kB–55 kB.

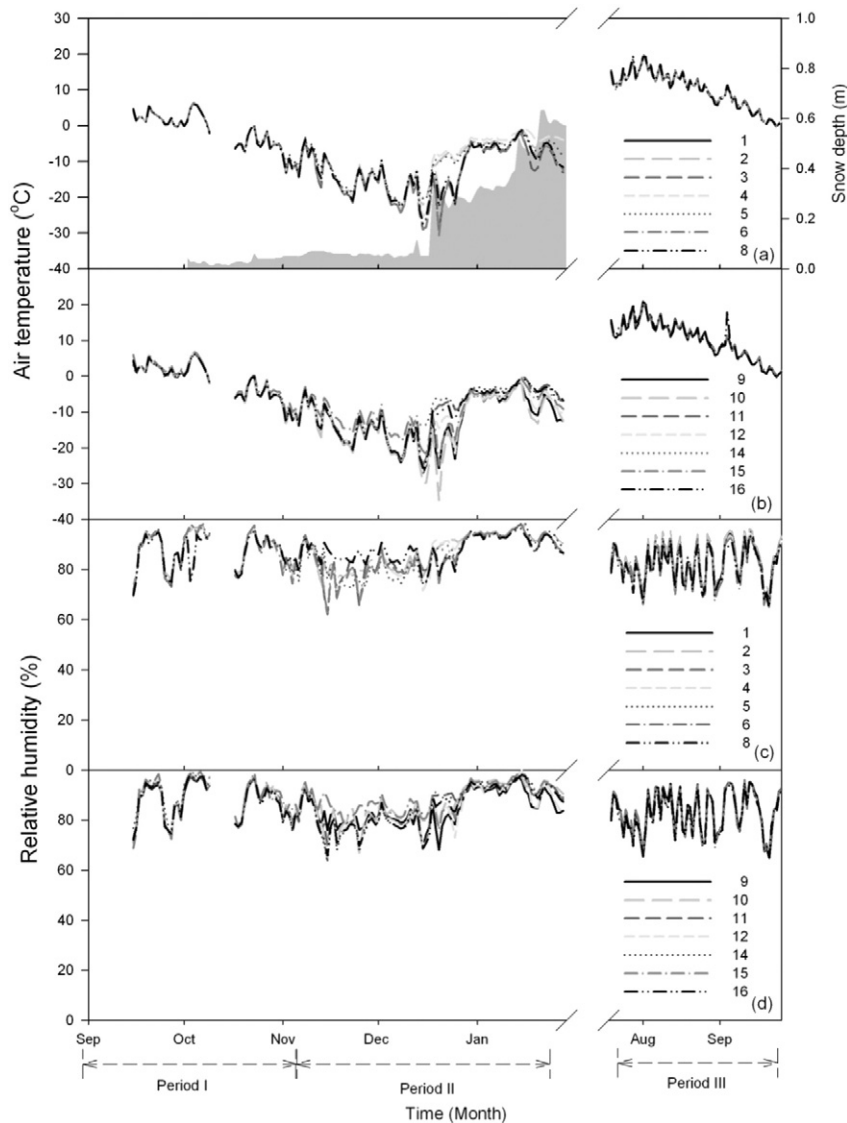


**Fig. 6.** Air temperature at eight locations (Nos. 1, 2, 3, 4, 5, 6, and 8) and snow depth from the weather system of IARC, UAF (a), air temperature at eight locations (Nos. 9, 10, 11, 12, 14, 15, and 16) (b), relative humidity at eight locations (Nos. 1, 2, 3, 4, 5, 6, and 8) (c), and relative humidity at eight locations (Nos. 9, 10, 11, 12, 14, 15, and 16) 0.1 m above the surface for periods I–III.

and near the chamber system plot. The net  $\text{CO}_2$  exchange was measured using an automated chamber system (Li840, LI-COR, Inc., Lincoln, NE, USA and manufactured chambers) at 15 locations in the  $\text{CO}_2$  flux measurement plot, and  $T_s$  was measured simultaneously at a depth of about 0.1 m below the soil surface from 6 July to 11 September, before period I.

## 4. Results

### 4.1. Air temperature ( $T_a$ ) and relative humidity (RH)

The daily average  $T_a$  0.1 m above the surface at the 16 measurement locations ranged from  $-35^\circ\text{C}$  to  $20^\circ\text{C}$  (Fig. 6a and b). The continuous  $T_a$  measurements for the periods were compared, except the values at Nos. 1, 7, and 13 for periods I–II and Nos. 7, 10, 11, 12, and 13 for period III due to communication errors caused by water leakage. Temporal variation in  $T_a$  showed no significant differences in magnitude over the study period as a whole ( $p > 0.05$ ; ANOVA) but did show significant differences in magnitude during period II ( $p < 0.05$ ; ANOVA). The daily average RH 0.1 m above the surface at 16 locations ranged from 62% to 99%

(Fig. 6c and d). The temporal variation in RH for all locations also showed significant differences in magnitude only during period II ( $p < 0.05$ ; ANOVA).

The  $T_a$  and RH values at all locations in the snow-free season were not different due to the atmospheric mixing caused by turbulence near the surface in the study plot. However,  $T_a$  and RH values in the snow-covered season, wherein some sensors were covered by snow, were different among the locations because the snow coverage and depth on the ground surface were affected by the distribution of vegetation (e.g., grass at a depth of around 0.3 m in the tussock, shrubs, moss, etc.) and by wind direction and speed. To verify the significant differences in  $T_a$  and RH in period II, snow depth data from the weather system of the International Arctic Research Center at the University of Alaska, Fairbanks were used (Fig. 6a). The temporal variations in  $T_a$  and RH corresponded with those of the accumulated snowfall. The magnitudes of  $T_a$  and RH were increased at several locations (e.g., Nos. 2, 4, 11, 12, and 12) and were then more or less constant when the snow accumulated to higher than 0.2 m after 17 December because accumulated snow layer protected near-surface sensors from cold air and strong wind as a buffer layer.

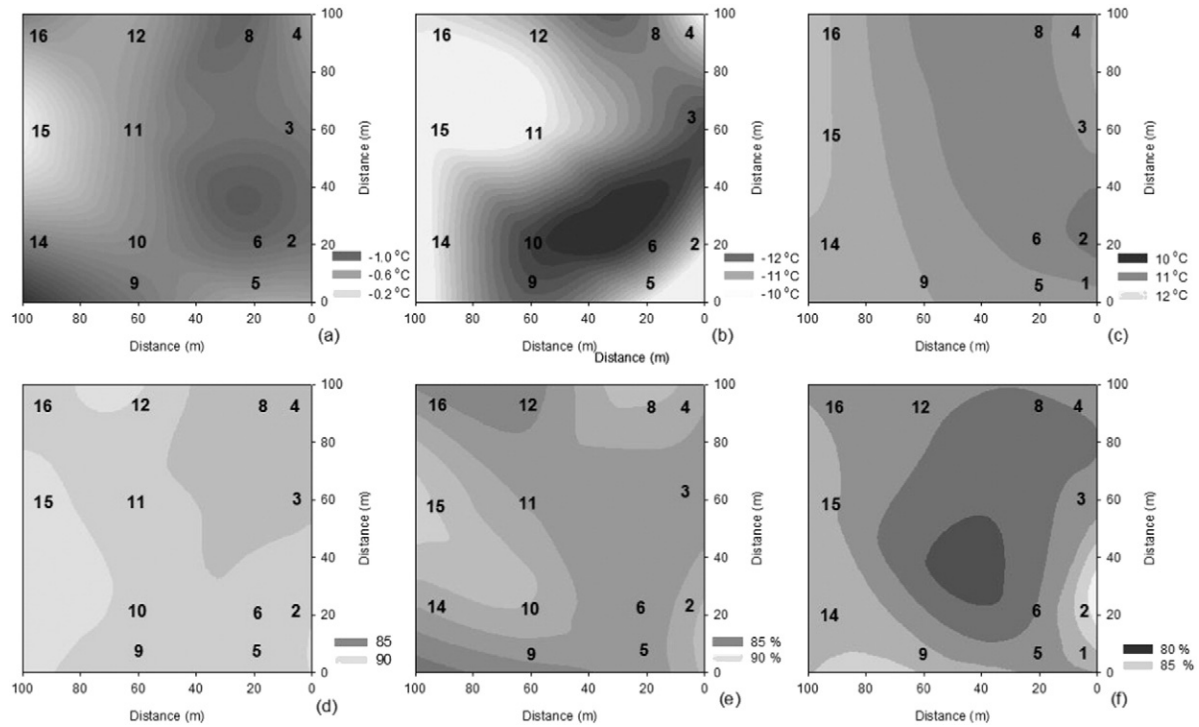


**Fig. 7.** Spatial distributions of the air temperature (a: period I; b: period II; and c: period III) at 11 or 13 locations, and relative humidity (d: period I; e: period II; and f: period III) at 12 or 13 locations in a 100 m × 100 m plot.

Fig. 7 shows the spatial distributions of average  $T_a$  (a, b, and c) and RH (d, e, and f) for period I (a and d), period II (b and e), and period III (c and f). The average  $T_a$  of each period ranged from  $-1.0$  °C (No. 8) to  $0.1$  °C (No. 15), from  $-12.8$  °C (No. 10) to  $-9.3$  °C (No. 14), and from  $10.9$  °C (No. 2) to  $11.5$  °C (No. 16), respectively (Fig. 7a, b, and c).  $T_a$  showed a wide range of spatial distribution for period II in winter (Fig. 7b). The average RH of each period ranged from 87 to 89%, from 85 to 88%, and from 82 to 85%, respectively (Fig. 7d, e, and f). The spatial patterns of  $T_a$  were similar in the three periods, within 2 °C, and those of RH were also not different, with only slight variation (5%).

#### 4.2. Soil temperature ( $T_s$ ) and soil water content (SWC)

The daily average  $T_s$  changed seasonally from around  $-10$  °C to  $10$  °C during the three periods (Fig. 8a and b). The  $T_s$  values at the 10 locations showed significant differences in magnitude for periods I–III ( $p < 0.05$ ; ANOVA).  $T_s$  decreased to less than  $0$  °C by mid-October, reached a minimum value near  $-10$  °C in mid-December, and then increased to near  $0$  °C in January due to the insulating effect of the snow cover. For period III,  $T_s$  showed a maximum value near  $10$  °C in early August and then gradually decreased.

The daily average SWC ranged from 3% to 50% (Fig. 8c and d). However, no sensor outputs except No. 1 recorded a measurement higher than 50% for period I due to limitations in sensor performance. The SWC decreased dramatically after 3 November 2012 and was then measured near 0% due to a deficiency in sensor type (i.e., time domain reflectometer, TDR) for measuring below-freezing temperatures. Therefore, although the SWC for period II was not properly measured, soil freezing was assumed based on the  $T_s$  for the same period. Based on the response of the SWC using the performance of TDR, the freezing stage and the freezing speed of the soil water were indirectly estimated for one month after 3 November. The SWC values in period III showed significant differences in two locations; it was less than 10% at location No. 1 due to the coarse humic layer, while that at location No. 10 was around 50% due to the downward slope. The other SWC values ranged from 20 to 40% during period III. The continuous SWC values at six

locations (Nos. 1, 3, 7, 8, 9, and 10) demonstrated significant differences in magnitude during period III ( $p < 0.05$ ; ANOVA).

Fig. 9 shows the spatial distribution of the average  $T_s$  for each period (a: period I, b: period II, and c: period III) and the average SWC for period III (d). The average  $T_s$  values ranged from  $0.7$  °C (No. 6) to  $1.3$  °C (No. 4) during period I, from  $-5.8$  °C (No. 2) to  $-2.5$  °C (No. 10) during period II, and from  $4.7$  °C (No. 3) to  $8.5$  °C (No. 1) during period III. The average SWC of the six locations ranged from 7% (No. 1) to 49% (No. 10) during period III. The spatial patterns of  $T_s$  also depended on the distribution of the vegetation and on the micro-topography, so the spatial patterns in the three periods were not similar. The  $T_s$  for period I had a very slight spatial variation due to its narrow range ( $\sim 0.6$  °C), while those for periods II and III had wide spatial variation. The difference between the spatial patterns of periods II and III was mainly caused by the heterogeneous distribution of the snow coverage and depth in period II, similar to  $T_a$  and RH. On the other hand, in the comparison of the spatial patterns of  $T_s$  and SWC, opposing patterns were observed at several locations (Nos. 1, 3, 8, and 10) in period III. This negative relationship between  $T_s$  and SWC was due to micro-topography with an upward or downward slope and a coarse humic layer.

#### 4.3. Coefficient of variation (CV)

The coefficient of variation (CV: ratio of the standard deviation to the mean) was used to evaluate the spatial variations in  $T_a$ , RH,  $T_s$ , and SWC. Fig. 10 shows the wide spatial variations in  $T_s$  and SWC according to the seasonal change of the CV. The CV of  $T_s$  ranged from 20 to 40% in period III, while that of SWC was about 40%. The CV of  $T_a$  was within 5% for periods I and III and increased by a maximum of 30% within the temperature range of  $-30$  to  $-20$  °C during period II. The CV of the RH was within 3%.

#### 4.4. Image data

Fig. 11 shows images of 10 locations captured by camera sensors between 24 July 2012 and 24 August 2012. Six cameras (Nos. 1, 2, 5, 8, 9, and 10) were installed to monitor phenology, considering four cardinal

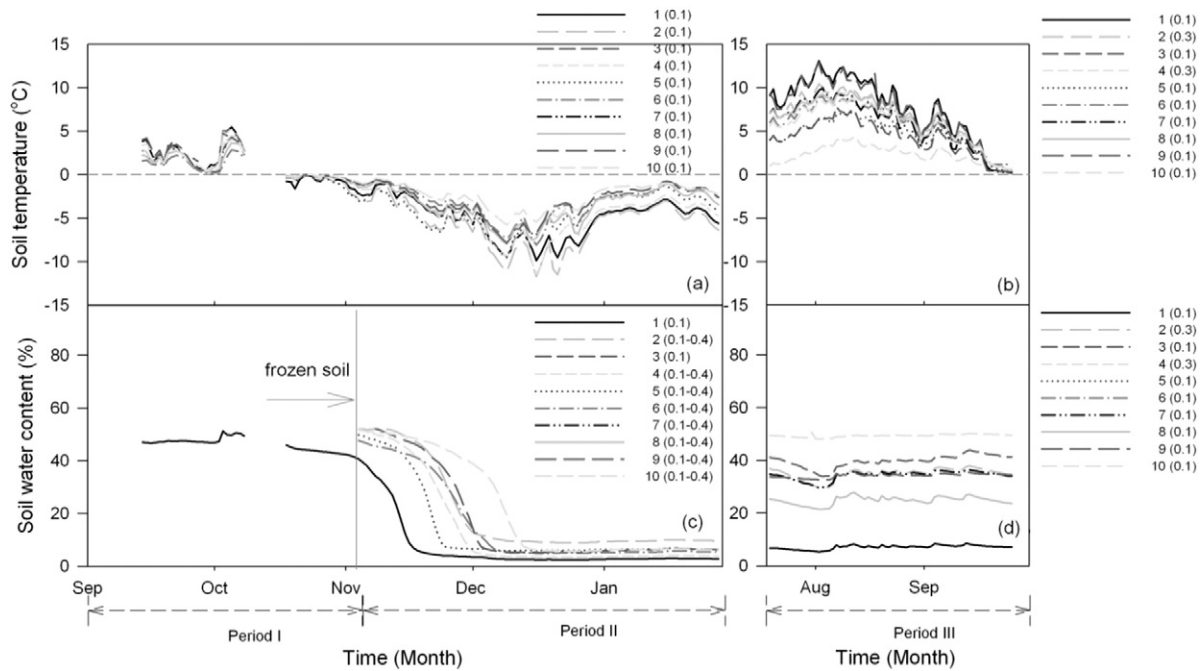


**Fig. 8.** (a) Soil temperature at a depth of 0.1 m in 10 locations for periods I and II. (b) Soil temperature at a depth of 0.1 m in eight locations (Nos. 1, 3, 5, 6, 7, 8, 9, and 10) and at a depth of 0.3 m in two locations (Nos. 2 and 4) for period III. (c) Soil water content at a depth of 0.1 m in two locations (Nos. 1 and 3) and in the 0.1–0.4 m layer in eight locations (Nos. 2, 4, 5, 6, 7, 8, 9, and 10) for periods I and II. (d) Soil water content at a depth of 0.1 m at eight locations (Nos. 1, 3, 5, 6, 7, 8, 9, and 10) and at a depth of 0.3 m in two locations (Nos. 2 and 4) for period III. Unit is meter.

points, and the other cameras (Nos. 3, 4, 6, and 7) were installed to monitor the growth of plants in the CO<sub>2</sub> chamber and to verify the operation of the chamber system. The image date could not be more accurately

investigated due to poor resolution of the phenology. Unfortunately, there was a limit to the real-time data transfer of high-resolution images as only one channel of Iridium was used.

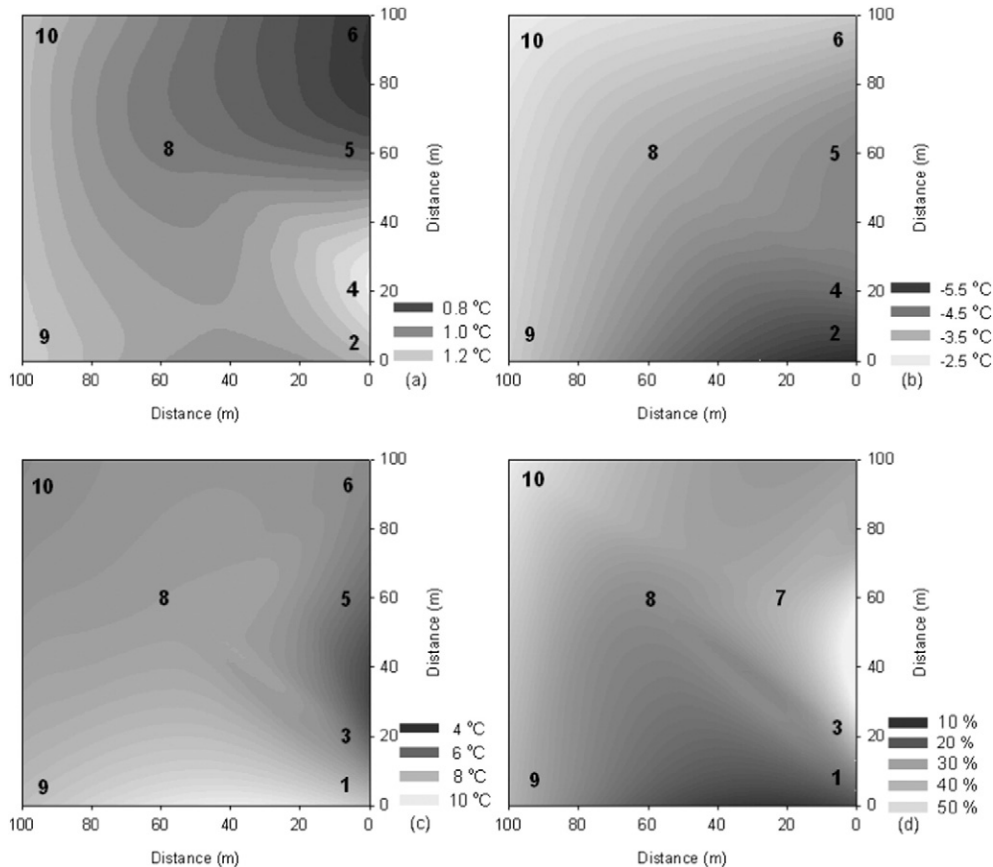


**Fig. 9.** Spatial distribution of the soil temperature at seven locations (Nos. 2, 4, 5, 6, 8, 9 and 10) for period I (a) and period II (b), spatial distribution of the soil temperature at seven locations (Nos. 1, 3, 5, 6, 8, 9, and 10) for period III (c), and soil water content at five locations (Nos. 1, 3, 7, 8, 9, and 10) for period III (d) in a 100 m × 100 m plot.

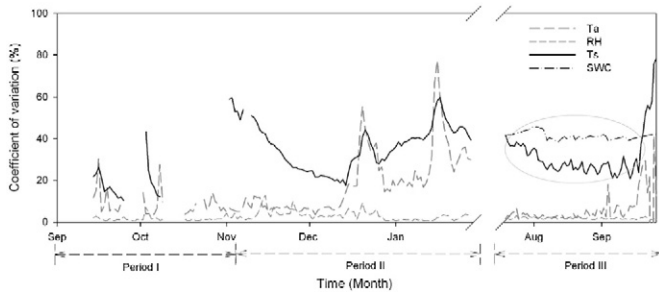


**Fig. 10.** Coefficients of variation of the soil temperature (Ts), soil water content (SWC), air temperature (Ta), and relative humidity (RH). The circle indicates high coefficients of variation in summer.

4.5. Estimation of soil CO<sub>2</sub> efflux

To estimate the spatial variation in soil CO<sub>2</sub> efflux in 2013, the relationship between soil CO<sub>2</sub> efflux and Ts or SWC showing high CV was examined. Nightly average net CO<sub>2</sub> exchange with Ts and SWC in 2012 was used to estimate soil CO<sub>2</sub> efflux in 2013. Equations for the exponential function (Eq. (1); Lloyd and Taylor, 1994) of Ts and the parabolic function (not shown) of SWC (Mielnick and Dugas, 2000) were used. The coefficients *a* and *b* were derived from non-linear least-square fittings (*a* > 0 and *b* > 0). However, a relationship between soil CO<sub>2</sub> efflux and Ts was found only under dry conditions (Fig. 12). The coefficients *a* and *b* were 0.066 and 0.1443, based on measurement data in 2012 (*R*<sup>2</sup> = 0.59). Soil CO<sub>2</sub> efflux in 2013 was calculated in the range of 0.08 mg m<sup>-2</sup> s<sup>-1</sup> to 0.47 mg m<sup>-2</sup> s<sup>-1</sup> for the same range of Ts based on the observed relationship (Fig. 13a). Fig. 13b shows the spatial distribution of estimated soil CO<sub>2</sub> efflux. The average soil CO<sub>2</sub> efflux for period III ranged from 0.09 mg m<sup>-2</sup> s<sup>-1</sup> (No. 4) to 0.19 mg m<sup>-2</sup> s<sup>-1</sup> (No. 9). The average CV of soil CO<sub>2</sub> efflux was 28%.

$$\text{Soil CO}_2 \text{ efflux} = a \exp^{bT_s} \tag{1}$$

5. Discussion and future developments

To elucidate the carbon cycle, the environmental parameters of the tundra ecosystem were measured in a 100 m × 100 m plot using the U-RMS with an optimized battery system. The Ts and SWC values at 10 locations and the Ta and RH at 16 locations were measured in real time, and their temporal and spatial variations were investigated. Temporal variation in Ts ranged from 0 °C to 5 °C in mid-September, was less than 0 °C at the end of October, reached the minimum at -10 °C at the end of December, gradually increased in January, and showed a maximum value in early August. The SWC range varied between 10% and 50% in each location in summer and was higher than 50% during the thawing season in the fall. Ta decreased from 5 °C in early September to 0 °C in mid-October, achieved its minimum around -30 °C by the end of December, gradually increased to up to 0 °C in January, and showed a maximum value in early August. The RH generally varied in range from 70% to 95%, except in winter. In the permafrost regions, the temporal variations in the environmental parameters in the soil and the near-surface depended on the thawing in summer and the freezing and snow cover in winter.

The spatial variations in Ts and SWC demonstrated significant change with a high CV (20–40%). There was no change in Ta and RH within 5% and 3% of the CV during the overall study period. However, the Ta and RH changed only in winter due to the spatially heterogeneous snow cover.

Temporal and spatial variations in Ts and SWC can be used to monitor the active layer of permafrost. The Ts and SWC variations are affected by the thawing of the active layer. Therefore, the monitoring of Ts and SWC variations can estimate the change in the active layer in the snow-free season. Both are provided as indispensable initial or forcing data in the carbon cycle model of the permafrost, used to understand the thawing mechanism of the active layer. In addition, the index of spatial variation will be used as supplementary information for scaling up environmental parameters. Moreover, in winter, the changes in temporal and spatial variation in Ta and RH of the near-surface were due to the effects of the snow cover. Therefore, snow depth variations will be estimated based on the temporal and spatial variations in Ta and RH



**Fig. 11.** Images for the monitoring of the chamber system and the phenology at 10 locations in 2012.

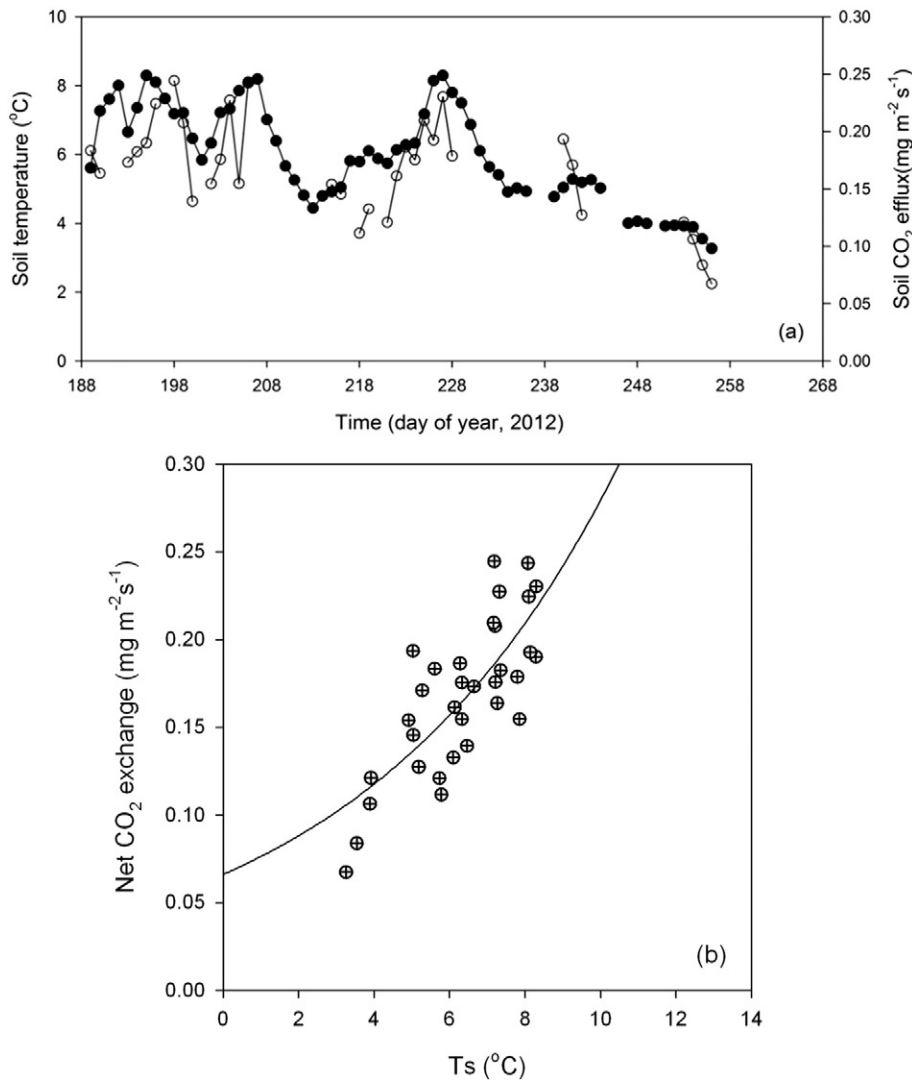


**Fig. 12.** (a) Temporal variation of soil temperature ( $T_s$ ) and soil  $\text{CO}_2$  efflux from July 6 to September 11 (from DOY 188 to DOY 255), 2012 (solid-circle line is  $T_s$ ; open-circle line is soil  $\text{CO}_2$  efflux). (b) Relationship between  $T_s$  and soil  $\text{CO}_2$  efflux.

when there is no snow-depth sensor (e.g., sonic ranging sensor) or when there is limited snowfall measurement.

Using the chamber system, soil  $\text{CO}_2$  efflux was measured with environmental parameters, using U-RMS in 2012. However, soil  $\text{CO}_2$  efflux was not measured in 2013. Therefore, an estimation of soil  $\text{CO}_2$  efflux during summer in 2013 was attempted based on the relationship between soil  $\text{CO}_2$  efflux and  $T_s$ , with high CV in 2012. The  $T_s$  explained ~60% of the variation in the soil  $\text{CO}_2$  efflux during summer. The soil  $\text{CO}_2$  efflux varied spatially by 25% of  $T_s$ , with a 28% CV. Emission from the soil surface is a major component of the surface carbon budget. The measurement of soil  $\text{CO}_2$  efflux in the polar region is more meaningful than in other regions due to the lack of vegetation. Therefore, the spatial and temporal changes in these environmental parameters, within or on the permafrost, play important roles in the carbon cycle during the thawing period.

In this study, U-RMS had shown several advantages of wireless functionality, long battery life, high spatial resolution, easy deployment, light weight, and need for minimal human interventions. Therefore, U-RMS can be regarded as very suitable for the observation of various parameters in large areas without electricity and no communication infrastructure. Moreover, this system can monitor not only seasonal, but also annual variations in continuous and real-time data. For the long-term monitoring of annual variations, the primary

lithium battery of sensor nodes must be replaced with rechargeable small solar cell batteries. Condensation within the case should also be prevented.

A high-resolution camera was planned for installation in the WSN system in order to establish a high-quality vegetation index at the monitoring site. A high-resolution camera interfaced with an Iridium modem and use of the multi-channel approach can guarantee reliable and fast data transfer from any location (Mohammad et al., 2004). Furthermore, to scale up the monitoring area and to add various environmental parameters, the network coverage must be extended with a multi-hop mesh network.

#### Acknowledgments

This study was supported by a National Research Foundation of Korea grant funded by the Korean government (MSIP) (NRF-C1ABA001-2011-0021063) (Title: Establishment of Circum Arctic Permafrost Environment Change Monitoring Network and Future Prediction Techniques (CAPEC Project, KOPRI PN15081)) and by the Human Resources Program in KETEP, granted financial resource from the MOTIE, Republic of Korea (No. 2015403020073). We gratefully acknowledge Dr. Larry Hinzman and Dr. Jessica Cherry for assistance with snowfall data.

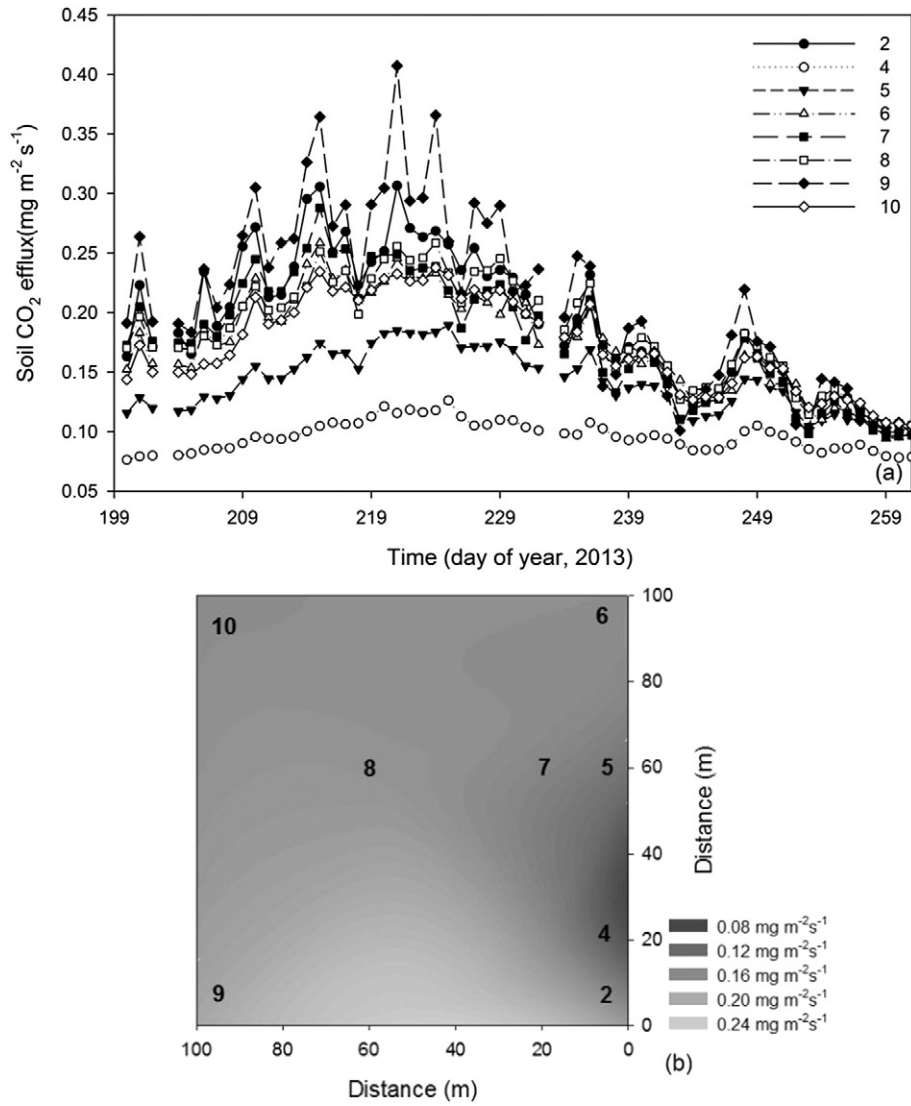


Fig. 13. (a) Temporal variation of the estimated soil CO<sub>2</sub> efflux at eight locations during period III. (b) Spatial distribution of the estimated soil CO<sub>2</sub> efflux at the same locations.

References

Albert, D.G., Decato, S.N., Carbee, D.L., 2008. Snow cover effects on acoustic sensors. *Cold Reg. Sci. Technol.* 52, 132–145.

Boone, R.D., Nadelhoffer, K.J., Canary, J.D., Kaye, J.P., 1998. Roots exert a strong influence on the temperature sensitivity of soil respiration. *Nature* 396, 570–572.

Davidson, E.A., Verchot, L.V., Cattanio, J.H., Ackerman, I.L., Carvalho, J.E.M., 2000. Effects of water content on soil respiration in forests and cattle pastures of eastern Amazonia. *Biogeochemistry* 48, 53–69.

Foken, T., Aubinet, M., Leuning, L., 2012. The eddy covariance method. In: Aubinet, M., Vesala, T., Papale, D. (Eds.), *Eddy Covariance*. Springer, New York, pp. 1–19.

Gill, K., Yang, S., Yao, F., Lu, X., 2009. A zigbee-based home automation system. *IEEE Trans. Consum. Electron.* 55, 422–430.

Gungor, V.C., Hancke, G.P., 2009. Industrial wireless sensor networks: challenges, design principles, and technical approaches. *IEEE Trans. Ind. Electron.* 56, 4258–4265.

Kotovirta, V., Karvonen, J., Bock und Polach, R., Berglund, R., Kujala, P., 2011. Ships as a sensor network to observe ice field properties. *Cold Reg. Sci. Technol.* 65, 359–371.

Lloyd, J., Taylor, J.A., 1994. On the temperature dependence of soil respiration. *Funct. Ecol.* 8, 315–323.

Mielnick, P.C., Dugas, W.A., 2000. Soil CO<sub>2</sub> flux in a tallgrass prairie. *Soil Biol. Biochem.* 32, 221–228.

Mohammad, A.J., Frost, V., Zaghoul, S., Prescott, G., Braaten, D., 2004. Multi-channel iridium communication system for polar field experiments. *Geoscience and Remote Sensing Symposium IGARSS '04. Proceedings. 2004 IEEE International 1*, pp. 121–124.

Nay, S.M., Mattson, K.G., Bormann, B.T., 1994. Biases of chamber methods for measuring soil CO<sub>2</sub> efflux demonstrated with a laboratory apparatus. *Ecology* 75, 2460–2463.

Oechel, W.C., Vourlitis, G.L., 1994. The effects of the climate change on land-atmosphere feedbacks in Arctic tundra regions. *Trends Ecol. Evol.* 9, 324–329.

Pewé, T.L., 1983. Alpine permafrost in the contiguous United States: a review. *Arct. Alp. Res.* 52, 145–156.

Rey, A., Pegoraro, E., Tedeschi, V., Parri, I., Jarvis, P.G., Valentini, R., 2002. Annual variation in soil respiration and its components in a coppice oak forest in central Italy. *Glob. Chang. Biol.* 8, 851–866.

Sardini, E., Serpelloni, M., 2011. Self-powered wireless sensor for air temperature and velocity measurements with energy harvesting capability. *IEEE Trans. Instrum. Meas.* 5, 1838–1844.

See, C.H., Horoshenkov, K.V., Abd-Alhameed, R.A., Hu, Y., Tait, S.J., 2012. A low power wireless sensor network for gully pot monitoring in urban catchments. *IEEE Sens. J.* 12, 1545–1553.

Spacek, A.D., Ando, O.H., Neto, J.M., Coello, V.L., Oliveira, M.O., Gruber, V., Schaeffer, L., 2013. Management of mechanical vibration and temperature in small wind turbines using zigbee wireless network. *Rev. IEEE Am. Lat.* 11, 512–517.

Swanson, R.V., Flanagan, L.B., 2001. Environmental regulation of carbon dioxide exchange at the forest floor in a boreal black spruce ecosystem. *Agric. For. Meteorol.* 108, 165–181.

Vilajosana, I., Lloja, J., Schaefer, M., Surinac, E., Vilajosana, X., 2011. Wireless sensors as a tool to explore avalanche internal dynamics: experiments at the Weissfluhjoch Snow Chute. *Cold Reg. Sci. Technol.* 65, 242–250.

Vourlitis, G.L., Oechel, W.C., Hastings, S.J., Jenkins, M.A., 1993. The effect of soil moisture and thaw depth on CH<sub>4</sub> flux from wet coastal tundra ecosystem on the North slope of Alaska. *Chemosphere* 26, 329–337.

Wang, D., Liao, W., 2006. Wireless transmission for health monitoring of large structures. *IEEE Trans. Instrum. Meas.* 55, 972–981.

Whelan, M.J., Gangone, M.V., Janoyan, K.D., 2009. Highway bridge assessment using an adaptive real-time wireless sensor network. *IEEE Sens. J.* 9, 1405–1413.

Zhang, T., Heginbottm, J.A., Barry, R.E., Brown, J., 2000. Further statistics on the distribution of permafrost and ground ice in the Northern Hemisphere. *Polar Geogr.* 24, 126–131.

ZigBee Standard Organization, 2007. *ZigBee Specification Document 053474r17*. pp. 12–13.